Mon. Not. R. Astron. Soc. **000**, 1–5 (2011) Printed 4 February 2011 (MN LATEX style file v2.2)

Evidence for a black hole in the X-ray transient XTE J1859+226

J. M. Corral-Santana[1,2] ⋆, J. Casares[1,2], T. Shahbaz[1,2], C. Zurita[1,2], I. G. Martínez-Pais[1,2], P. Rodríguez-Gil[3,1,2]

[1] *Instituto de Astrofísica de Canarias (IAC), Vía Láctea s/n, La Laguna E-38205, S/C de Tenerife, Spain*
[2] *Departamento de Astrofísica, Universidad de La Laguna, La Laguna E-38205, S/C de Tenerife, Spain*
[3] *Isaac Newton Group of Telescopes, Apartado de Correos 321, Santa Cruz de La Palma E-38700, Spain*

Accepted 2011 January 31.

ABSTRACT

We present the results of time-resolved optical photometry and spectroscopy of the X-ray transient XTE J1859+226 (V406 Vul). Photometric observations taken during 2000 and 2008 reveals the presence of the secondary star's ellipsoidal modulation. Further photometry obtained in 2010 shows the system ≃1 mag brighter than its quiescence level and the ellipsoidal modulation diluted by strong flaring activity. Spectroscopic data obtained with the 10.4-m GTC in 2010 reveals radial velocity variations of $\sim 500\,\mathrm{km\,s^{-1}}$ over 3 h. A simultaneous fit to the photometry and spectroscopy using sinusoids to represent the secondary star's ellipsoidal and radial velocity variations, yields an orbital period of 6.58 ± 0.05 h and a secondary star's radial velocity semi-amplitude of $K_2 = 541 \pm 70\,\mathrm{km\,s^{-1}}$. The implied mass function is $f(M) = 4.5 \pm 0.6\,\mathrm{M_\odot}$, significantly lower than previously reported but consistent with the presence of a black hole in XTE J1859+226. The lack of eclipses sets an upper limit to the inclination of 70 degrees which yields a lower limit to the black hole mass of $5.42\,\mathrm{M_\odot}$.

Key words: Accretion, accretion disks, binaries: close, stars: individual: XTE J1859+226 (=V406 Vul), X-rays: binaries

1 INTRODUCTION

The mass distribution of compact objects has crucial impact on fundamental physics, and can only be determined from the study of X-ray binaries (Charles & Coe 2006; Casares 2007). In particular, the theoretical black-hole (BH) and neutron star (NS) mass distributions depend critically on the equation of state (which establishes the critical mass dividing NS and BH formation) and on our current understanding of the late stages in the evolution of massive stars and supernovae. The latter contains several theoretical uncertainties which completely dominate the final mass distribution (e.g. treatment of convective mixing, amount of fall-back, mass-cut, mass-loss during Wolf-Rayet phase, initial mass function of progenitors, etc; see e.g. Fryer & Kalogera 2001). It should be noted that the upper mass cut-off of the BH distribution is particularly constraining (Orosz & et al. 2007).

⋆ E-mail: jcorral@iac.es (JMC-S), jcv@iac.es (JC), tsh@iac.es (TS), czurita@iac.es (CZ), igm@iac.es (IGM-P), prguez@iac.es (PR-G)

Only 16 systems out of an estimated Galactic population of $\sim 10^3$ transient X-ray binaries have reliable dynamical mass determinations (e.g. Casares 2010). The typical error bars in BH mass measurements are ∼40 per cent and it is clear that more BH discoveries and a factor 2-3 improvement is needed before any constraints can be set on supernovae models (Bailyn et al. 1998; Özel et al. 2010). The mass determination in X-ray binaries requires knowledge of the radial velocity curve, the binary mass ratio and the orbital inclination (the latter from modelling the tidally distorted companion's light curve).

XTE J1859+226 was discovered during its 1999 outburst (Wood et al. 1999) and its X-ray properties promptly classified it as a BH candidate. Orbital periods of 6.72 h (Uemura et al. 1999), 9.12 h (Garnavich et al. 1999) and 18.72 h (McClintock et al. 2000) were reported although none of them could be confirmed. Finally, data taken in quiescence (Zurita & et al., 2002) during September and November 2000 (in 4 night snapshots of 1.5 h-4 h duration) exhibited a ∼0.2 mag semi-amplitude sinusoidal modulation, consistent with an secondary star's ellipsoidal variation (caused by the changing visibility of the tidally distorted

companion star as it orbits the compact object). The periodogram of this modulation suggests that periods from 6.6 to 11.2 h are equally possible at the 68 per cent confidence level. On the other hand, Filippenko & Chornock (2001) report a preliminary analysis of radial velocities based on 10 spectra obtained over two nights. They claim evidence for a sinusoidal variation with a period of 9.1 h and companion radial velocity semi-amplitude $K_2 = 570 \pm 27\,\mathrm{km\,s^{-1}}$. The implied mass function is $f(M) = 7.4 \pm 1.1$ M$_\odot$, one of the largest ever measured making J1859+226 a very promising massive BH. Although this result has been used by other authors, it should be noted that it has never been published in a refereed journal and hence we believe these parameters require confirmation. Therefore, we have embarked on a photometric and spectroscopic campaign with the aim of determining the orbital period of the binary and its dynamical mass function.

2 OBSERVATIONS AND DATA REDUCTION

2.1 Photometry

XTE J1859+226 was observed on 2008 July 31-August 1 and 2010 July 13-14 using ALFOSC at the 2.5-m Nordic Optical Telescope (NOT) in the *R*-band. The conditions for the 2008 campaign were affected by thick dust (calima) and therefore we decided to use long integration times. Eight 1800-s images were obtained on the night of July 31 and thirteen 900-s images on August 1, covering ∼5-7 h per night. The 2010 campaign was performed under excellent seeing (∼0.5 arcsec) and transparency conditions, so shorter exposure times were adopted. Twenty two and thirty two 800-s integrations were obtained on the nights of July 13-14 respectively, covering ∼8 h per night. XTE J1859+226 was also observed on the night of 2010 August 8 using ACAM at the 4.2-m William Herschel Telescope (WHT). A total of 147 frames were obtained in the *R*-band using 120-s integration time for ∼6.5 h. All the images were corrected for bias and flat-fielded with `IRAF` in the standard way. Aperture photometry was then performed on the object and the five comparison stars reported in Zurita & et al., (2002).

2.2 Spectroscopy

Optical spectroscopy of XTE J1859+226 was obtained on the nights of 2010 July 17 and August 13 using OSIRIS at the 10.4-m Gran Telescopio Canarias (GTC). Five 1900-s spectra were obtained every night using the R1000B grism and a 0.6-arcsec slit, which provides a wavelength coverage of $\lambda\lambda$3630-7500 at 255 km s^{-1} resolution (FWHM). The radial velocity standards 61 Cyg A & B were also observed during the second run using an identical set up. A Hg-Ar-Ne arc was obtained with the telescope in park position to provide the wavelength calibration scale. Standard procedures were used to de-bias and flat-field the spectra. The 1-dimensional spectra were extracted using optimal extraction routines which maximize the final signal-to-noise ratio. The wavelength calibration, flux calibration and radial velocity analysis were made with `MOLLY`[1]. The wavelength calibration was obtained using a fourth-order polynomial fit to 34 arc lines resulting in a dispersion of 2.14 Å pix^{-1} and a rms scatter of 0.07 Å. The instrumental flexure was monitored by measuring the position of the sky line OI 5577.340Å which was used to correct the individual spectra. The spectra were also calibrated in flux using observations of the flux standard GL57-34.

[1] http://www.warwick.ac.uk/go/trmarsh/software

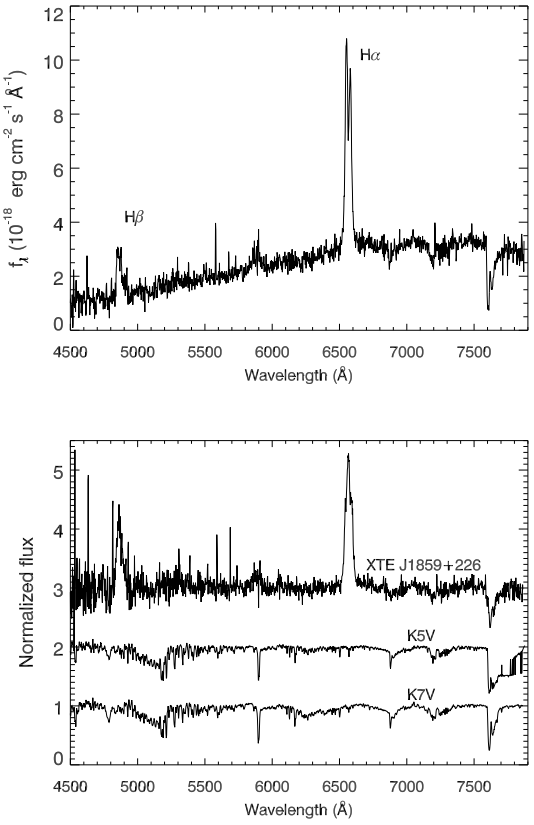

Figure 1. Top: the average optical spectrum of XTE J1859+226. A red continuum with broad double-peaked emission lines of Hα and Hβ are clearly present. The feature at ∼5890 Å is possibly associated to HeI emission. **Bottom:** Comparison of the Doppler corrected average of J1859+226 with the two observed templates. The spectra have been rectified to the continuum and offset vertically for the sake of clarity.

3 OVERVIEW OF OPTICAL PHOTOMETRY AND SPECTROSCOPY

3.1 Spectroscopy

The top panel in Fig. 1 shows the flux-calibrated average spectrum of XTE J1859+226. It shows a red continuum with broad double-peaked emission lines at the positions of Hα and Hβ, characteristic of X-ray transients in quiescence. The Hα line has a typical equivalent width of ≃130 Å and FWHM≃2340 km s^{-1}. The individual spectra of XTE J1859+226 and the template stars 61 Cyg A and B were prepared for the cross-correlation analysis by subtracting of a low-order spline fit to the continuum, after masking the Hα and Hβ emission lines and atmospheric absorption features. The spectra were then rebinned onto a uniform

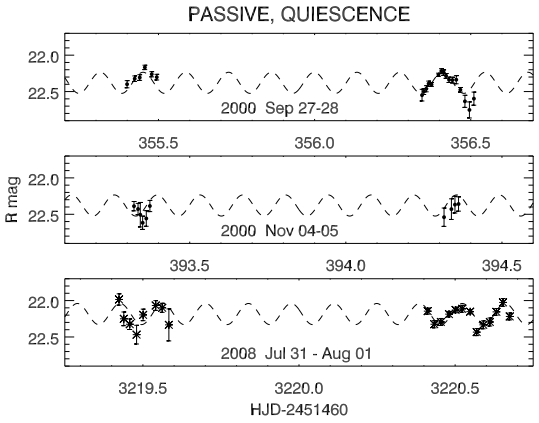

Figure 2. ***Top & middle panels:*** Zurita et al. (2002) epoch C optical photometry taken in 2000. ***Bottom:*** Optical photometry taken in 2008 July 31 and August 1 showing the dominance of the ellipsoidal modulation. The solid line is the simulated secondary star's ellipsoidal modulation determined in section 4. Passive refers to the "true" quiescence state as defined by Cantrell & Bailyn (2007).

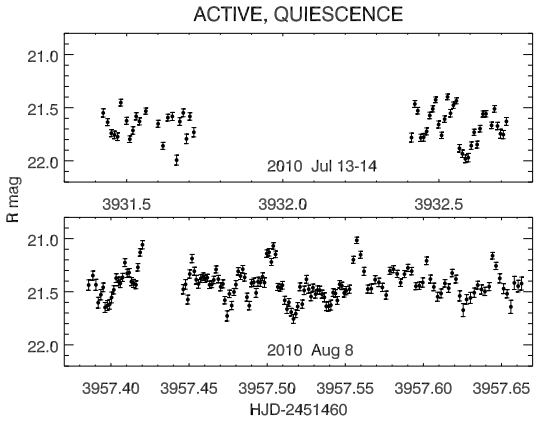

Figure 3. The optical photometry of XTE J1859+226 taken on 2010 July 13-14 using the NOT (top) and August 8 using the WHT (bottom). The short 120-s integration time of the WHT images enables us to resolve the flickering activity which strongly dilutes the secondary star's ellipsoidal modulation. Active refers to the flickering state as defined by Cantrell & Bailyn (2007).

velocity scale of 112 km s^{-1} per pixel and the unit continuum was subtracted. Cross-correlation between the target spectrum and the K5V template 61 Cyg A was then performed in the region 5000-6516 Å after masking the atmospheric and interstellar feature at $\lambda\lambda$6285-6310 and the bump at ∼5890 Å, possibly associated to HeI emission. Radial velocities were extracted by fitting parabolic functions to the cross-correlation peaks. Clear velocity excursions of a few hundred km s^{-1} are seen on each night. We note that the radial velocities are not significantly affected by the choice of either a K5V or K7V template. However, in an attempt to constrain the spectral type we have performed an optimal subtraction analysis of the Doppler corrected average of J1859+226 (using the orbital solution reported in section 4) with the 2 templates (see e.g. Marsh, Robinson & Wood 1994). The χ^2 of the residual slightly favours the K5V template, with 928 versus 944 for 742 degrees of freedom. The bottom panel of Fig. 1 displays the Doppler corrected average and the 2 templates. Although the spectrum is too noisy to make a direct comparison of the metallic absorption lines, the relative depth of the broad CaH and TiO bands at 6300, 6800 and 7200 Å also supports the K5V versus the K7V spectrum.

3.2 Photometry

The light curves of XTE J1859+226 were determined through differential photometry using 5 comparison stars (see Zurita & et al., 2002) as local standards. Zurita & et al., (2002) report a quiescent magnitude R=22.48±0.07 but we note that the target is brighter in our photometric campaigns by ∼0.25 mag in 2008 and ∼0.8-1.0 mag in 2010. The 2008 data clearly shows an ellipsoidal modulation (Fig. 2), caused by the tidal and rotational distortion of the companion star (e.g. see Cen X-4 in Shahbaz et al. 1993). However, the 2010 light curves show considerable scatter due to the presence of strong aperiodic variability which distorts the underlying ellipsoidal modulation: the flickering activity is most prominent in the 2010 August data (Fig. 3, bottom panel) compared with the 2010 July campaign (Fig. 3, top panel). This is probably due to the shorter integration times which enables us to resolve the individual flare events. It is also when XTE J1859+226 is brighter, about 1 mag above quiescence, so it is possible that the level of aperiodic variability correlates with the target brightness. A similar behaviour is seen in the black hole binary A0620-00, where flickering is found to decrease with magnitude (Cantrell et al. 2008; Cantrell & et al., 2010).

The light curves of quiescent X-ray binaries are known to be contaminated by optical flickering with time-scale of minutes to hours and amplitudes in the range 0.06-0.6 mag (Zurita, Casares & Shahbaz 2003, Hynes et al. 2003; Shahbaz et al. 2005, 2010). For comparison, the flares in XTE J1859+226 have a characteristic time-scale of ∼10 min and amplitudes up to 0.5 mag. Therefore, for the sake of constraining the orbital period (see section 4) we decided to restrict our analysis to the 2008 campaign, when the target was closer to its quiescent level and showed minimum flickering activity (the *passive* state as defined by Cantrell & Bailyn 2007). These data were also combined with quiescent photometry obtained in 2000 and reported in Zurita & et al., (2002). Both datasets were detrended by subtracting the nightly mean value.

4 PERIOD ANALYSIS AND DETERMINATION OF ORBITAL PARAMETERS

To determine the orbital period of XTE J1859+226 we compute a χ^2 periodogram using a prior knowledge about the expected modulations observed in the binary system. For a fixed frequency, we simultaneously fit the photometric light curve (32 and 21 data points from the 2000 and 2008 campaigns respectively; N_{LC}) and the radial velocity curve (10

data points; N_{RV}) with a model to represent the photometric and radial velocity variations. The photometric ellipsoidal modulation is equivalent to sinusoid of frequency $2f$ (where f is the orbital frequency) which lags by 90 degrees in phase relative to a sinusoid at frequency f. Although the light curves were taken when the system was in the "passive quiescent" state, there is the possibility that the accretion disc contribution was not the same for the two epochs, and so the light curves will have different amplitudes. To account for the different amplitudes we first fit the light curve of Zurita & et al., (2002) and then fit a scaled version of this to the data taken in our 2008 campaign. The radial velocity motions of the secondary star can be modelled with a sinusoid at frequency f. The phasing of the light curve and radial velocity curve are related and so the free model parameters are the orbital frequency, phase offset, the semi-amplitudes of the three sinusoids, the scale factor to account for the different disc contamination between the light curves, the magnitude offset for the light curve and the systemic velocity for the radial velocity curve.

Although the Nyquist frequency sets the maximum frequency we can theoretically search, inspection of the radial velocity curve shows a smooth modulation lasting more than 2 h and so any period we expect to detect should be longer than this. Given that observations are taken throughout entire and consecutive nights, the minimum frequency is limited to 24 h. Hence we limit our frequency search in the range 2 to 6 cycles d^{-1} with a total of 126 frequency steps ($2\times N_T$; where N_T=N_{LC}+N_{RV}=63 is the total number of data points; Press 2002). Given that there are two different types of data with different number of data points, to optimise the fitting procedure we assigned relative weights to the different data sets. After our initial search of the parameter space, which resulted in a good solution, we scaled the uncertainties on each data set (i.e., the light curve and the radial velocity curve) so that the total reduced χ^2 of the fit was $\approx$1 for each data set separately. After the scaling, the fitting procedure were run again to produce the final set of parameters. The 99 per cent white noise significance levels was estimated using Monte Carlo simulations. We generated light curves and radial velocities with exactly the same sampling and integration times as the real data, added Gaussian noise using the errors on the data points. We computed 5000 simulated light curves and then calculated the 99 per cent confidence level at each frequency taking into account a realistic number of independent trial (Vaughan 2005).

Three minima above the noise level are clearly seen at 3.65, 5.21 and 2.69 cycles d^{-1} (see Fig. 4, bottom panel). However, the best fit has a χ^2 of 54.7 (with 56 degrees of freedom) and occurs at a frequency of 3.65 cycles d^{-1}. The best fitted radial velocity parameters for this period are listed in Table 1. Note that the K_2 velocity, combined with the orbital period, implies a mass function $f(M) = K_2^3\,P/2\pi G = 4.5 \pm 0.6\,\mathrm{M}_\odot$ and hence the dynamical confirmation of a black hole. The next best fit at 5.21 cycles d^{-1} is only significant at the 3×10^{-4} per cent level and the remaining peak at 2.69 cycles d^{-1} (i.e. the $\sim$ 9.1 h period reported by Filippenko & Chornock 2001) has an even lower significance. The top panel in Fig. 4 shows the photometric light curve and radial velocity curve, folded on the 0.274 d period and with the best fitted solution superimposed. The peak-to-peak amplitude of the light curve of (Zurita & et al., 2002) is 0.239 mag and the difference between minima is 0.058 mag. The scale factor between the amplitudes of the two light curves is 0.84±0.20 which implies that within the uncertainties, the two light curves have similar amplitudes and disc contribution.

P (d)	K_2 (km s^{-1})	T_0 (HJD-2455000)	γ_0 (km s^{-1})
0.274 ± 0.002	541 ± 70	395.689 ± 0.002	-28 ± 53

Table 1. List of the best fitted radial velocity parameters obtained for XTE J1859+226

The relatively large amplitude of the light curve and the possible difference between the minima (where the minimum at phase 0.5 is deeper than the minimum at phase 0.0) places strong constraints on the binary inclination angle. Using our X-ray binary model which predicts the light curve arising from a Roche-lobe filling in an X-ray binary (Shahbaz et al. 2003) we find that systems with inclination angles of $\sim$40 degrees have equal minima. Furthermore, the lack of eclipses gives an upper limit of $\sim$70 degrees, which implies a lower limit in the mass of the black hole of 5.42 $\mathrm{M}_\odot$. Our data are not sufficiently accurate to allow a detailed analysis of the inclination angle, but we can use the X-ray binary model to estimate the distance and inclination angle. We assume a secondary star with an effective temperature similar to that in A0620-00 (an X-ray transient with a K4V secondary star with an orbital period of 7.8 h; see Marsh, Robinson & Wood 1994), E(B-V)=0.58 (Hynes et al. 2002) and the orbital parameters derived in section 3. We find that to reproduce the large amplitude of the flux level of the observed light curve requires a system at 14 kpc with an inclination angle of 60 degrees and no accretion disc contribution, or a system with an inclination angle of 70 degrees but with a disc contribution of 28%. We note in passing that the Galactic rotation velocity at this distance is $\simeq -53\,\mathrm{km\,s^{-1}}$ (Clemens 1985) which is consistent with the observed systemic velocity listed in Table 1. Clearly a more accurate light curve is required before we can place tight constraints on the model parameters.

5 CONCLUSION

We have presented R-band photometry of XTE J1859+226 obtained in 2008 and 2010. The 2008 light curves are dominated by the classical ellipsoidal modulation. However, the target is $\simeq$0.6–1 mag brighter than its quiescent level during 2010 and the secondary star's ellipsoidal modulation is found to be strongly diluted by the flickering activity. A χ^2 periodogram analysis combining the radial velocities and the quiescent photometry yields an orbital period of 6.58 ± 0.05 h (lower than previous claims by Filippenko & Chornock 2001) and a velocity semi-amplitude $541 \pm 70\,\mathrm{km\,s^{-1}}$. The implied mass function is $4.5 \pm 0.6\,\mathrm{M}_\odot$ substantially lower than reported in Filippenko & Chornock (2001), but still consistent with the presence of a black hole. More observations are required to further refine the orbital parameters of XTE J1859+226, in particular, the mass function.

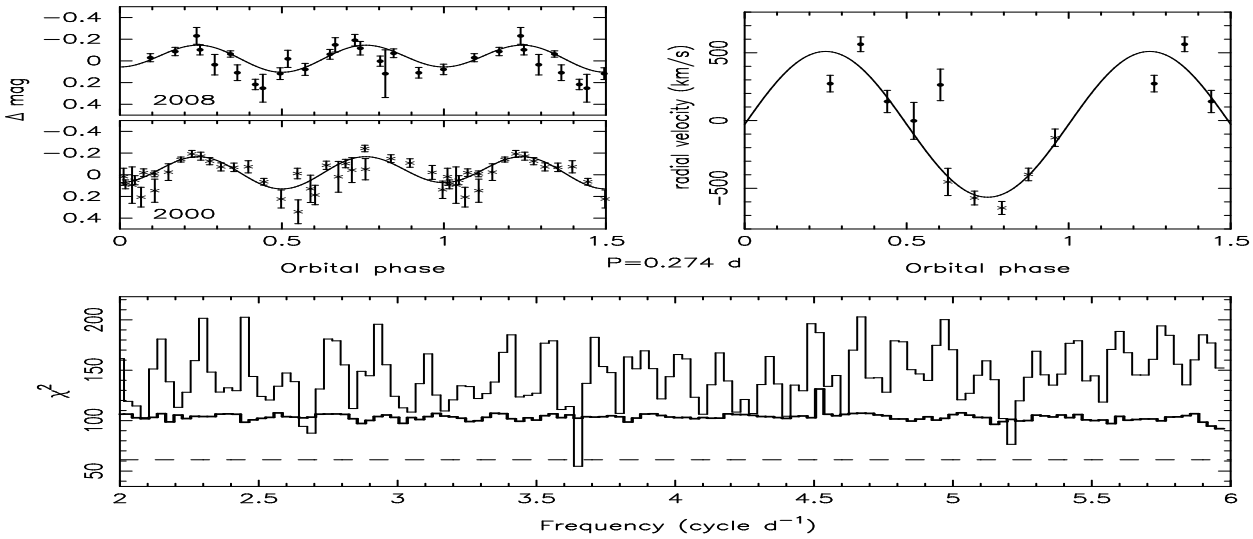

Figure 4. ***Bottom:*** The χ^2 periodogram. The solid line represents the 99 per cent white noise significance levels. The dashed line shows the 99 per cent confidence level above the minimum χ^2 at a frequency of 3.65 cycles d^{-1} (=0.274 d). ***Top left and right:*** Respectively, the optical photometric light curve and radial velocity curve phase folded on the best fit period. 1.5 orbital cycles are shown for clarity. In the radial velocity curve plot, the filled circles and stars show the data taken on different nights. In the top light curve plot the filled circles are the data from 2008, whereas in the bottom light curve plot the stars are the data from Zurita et al. (2002). The solid line in the plots show the best fit model using a double and single sinusoid to simulate the secondary star's ellipsoidal and radial velocity variations (see section 4).

ACKNOWLEDGEMENTS

The use of Tom Marsh's `MOLLY` package is gratefully acknowledge. The WHT is operated by the Isaac Newton Group (ING). The NOT is operated jointly by Denmark, Finland, Iceland, Norway, and Sweden. Both telescopes together with the Gran Telescopio Canarias (GTC) are installed in the Spanish Observatorio del Roque de los Muchachos of the Instituto de Astrofísica de Canarias (IAC), in the island of La Palma. We acknowledge support from the Spanish Ministry of Science and Innovation (MICINN) under the grant AYA 2007–66887. This program is also partially funded by the Spanish MICINN under the Consolider-Ingenio 2010 Program grant CSD2006-00070: "First Science with the GTC (http://www.iac.es/consolider-ingenio-gtc)". Based on observations made with the WHT Telescope on 2010 August 8 under the Spanish Instituto de Astrofísica de Canarias Director's Discretionary Time

REFERENCES

Bailyn C. D., Jain R. K., Coppi P., Orosz J. A., 1998, *ApJ*, 499, 367
Cantrell A. G., Bailyn C. D., 2007, *ApJ*, 670, 727
Cantrell A. G., Bailyn C. D., McClintock J. E., Orosz J. A., 2008, *ApJL*, 673, L159
Cantrell A. G., et al., 2010, *ApJ*, 710, 1127
Casares J., 2007, in Karas V., Matt G., eds, IAU Symp. Vol. 238, Black holes: from stars to galaxies - across the range of masses.. Cambridge University Press, pp 3–12
Casares J., 2010, in J. M. Diego L. J. Goicoechea J. I. G.-S., Gorgas J., eds, Highlights of Spanish Astrophysics V. Springer-Verlag, pp 3–14
Charles P. A., Coe M. J., 2006, Compact Stellar X-ray Sources. Cambridge University Press, pp 215–265
Clemens D. P., 1985, *ApJ*, 295, 422
Filippenko A. V., Chornock R., 2001, *IAU Circ.*, 7644, 2
Fryer C. L., Kalogera V., 2001, *ApJ*, 554, 548
Garnavich P. M., Stanek K. Z., Berlind P., 1999, *IAU Circ.*, 7276, 1
Hynes R. I., Charles P. A., Casares J., Haswell C. A., Zurita C., Shahbaz T., 2003, *MNRAS*, 340, 447
Hynes R. I., Haswell C. A., Chaty S., Shrader C. R., Cui W., 2002, *MNRAS*, 331, 169
Marsh T. R., Robinson E. L., Wood J. H., 1994, *MNRAS*, 266, 137
McClintock J. E., Remillard R. A., Heindl W. A., Tomsick J. A., 2000, *IAU Circ.*, 7466, 1
Orosz J. A., et al. 2007, *Nat.*, 449, 872
Özel F., Psaltis D., Narayan R., McClintock J. E., 2010, *ApJ*, 725, 1918
Press W. H., 2002, Numerical recipes in C++ : the art of scientific computing. Cambridge University Press
Shahbaz T., Dhillon V. S., Marsh T. R., Casares J., Zurita C., Charles P. A., 2010, *MNRAS*, 403, 2167
Shahbaz T., Dhillon V. S., Marsh T. R., Casares J., Zurita C., Charles P. A., Haswell C. A., Hynes R. I., 2005, *MNRAS*, 362, 975
Shahbaz T., Naylor T., Charles P. A., 1993, *MNRAS*, 265, 655
Shahbaz T., Zurita C., Casares J., Dubus G., Charles P. A., Wagner R. M., Ryan E., 2003, *ApJ*, 585, 443
Uemura M., Kato T., Pavlenko E., Shugarov S., Mitskevich M., 1999, *IAU Circ.*, 7303, 2
Vaughan S., 2005, *A&A*, 431, 391
Wood A., Smith D. A., Marshall F. E., Swank J., 1999, *IAU Circ.*, 7274, 1
Zurita et al., 2002, *MNRAS*, 334, 999
Zurita C., Casares J., Shahbaz T., 2003, *ApJ*, 582, 369